FINAL REPORT

1 General Information

DFG reference number: BA 5656/1-2 and WE 2623/14-2

Project number: 322462997

Project title: Microscopic understanding of disorder induced ferromagnetism in B2-alloy thin films II (MUMAGI II)

Name(s) of the applicant(s):

Dr. Rantej Bali, Scientific Staff, Helmholtz-Zentrum Dresden-Rossendorf, permanent

Dr. Heiko Wende, Professor, University of Duisburg-Essen, permanent

Name(s) of the cooperation partners:

Dr. Thomas Thomson, Professor, Manchester University UK

Dr. Yanning Zhang, Professor, UESTC, China

Reporting period (entire funding period):

27.07.2020 – 18.10.2024

2 Summary

MUMAGI II dealt with the investigation of ferromagnetic onsets in prototype binary alloy systems. A ferromagnetic onset can be triggered in a paramagnetic or anti-ferromagnetic system through changes to the lattice ordering.

In the first funding round (2017 – 2020), ferromagnetic onsets driven by chemical disordering in B2 $Fe_{60}Al_{40}$ as well as static disorder in B2 $Fe_{50}Rh_{50}$ were explored through comprehensive structural, magnetometry as well as spectroscopic observations. In the second funding round (2020 – 2024), the knowhow was exploited, for instance to generate nanoscale magnetic modulations over large areas using chemical as well as static disorder, and for *in situ* tracking of anomalous Hall resistivity during chemical disordering.

Furthermore, a different path to realizing ferromagnetic onsets was demonstrated, where instead of disordering, the lattice ordering of an initially short-range ordered $Fe_{60}V_{40}$ alloy film generates ferromagnetism. Regardless of the lattice (dis)ordering path, the ferromagnetic onsets can be triggered either by ion-irradiation or by single femtosecond laser pulses, thus the regions possessing the onsets are spatially confined to the respective ion/photon-matter interaction volumes.

A broad picture emerges, where several pathways for realizing ferromagnetic onsets are exploited for applications such as nanoscale magnetic patterning and spin-transport, as well as

for obtaining fundamental insights into the correlation between the atomic arrangement and the magnetic behaviour, providing the impulse for discovering further alloy systems for magnetic manipulation through atomic displacements.

Zusammenfassung

MUMAGI II befasste sich mit der Untersuchung ferromagnetischer Ordnungsbildung in prototypischen binären Legierungssystemen. Ferromagnetismus kann in einem paramagnetischen oder antiferromagnetischen System durch Änderungen der Gitterordnung entstehen.

In der ersten Förderperiode (2017 – 2020) wurde die ferromagnetische Ordnungsbildung, die durch strukturelle, chemische Unordnung in B2 $Fe_{60}Al_{40}$ sowie statische Unordnung in B2 $Fe_{50}Rh_{50}$ verursacht werden, durch umfassende strukturelle, magnetische und spektroskopische Beobachtungen erforscht. In der zweiten Förderperiode (2020 – 2024) wurde das gewonnene Know-how genutzt, um beispielsweise nanoskalige magnetische Modulationen über große Flächen mittels chemischer und statischer Unordnung zu erzeugen und den anomalen Hall-Widerstand während chemischer Unordnung in-situ zu verfolgen.

Darüber hinaus wurde ein alternativer Ansatz demonstriert, bei dem die Ordnung des Gitters eines zunächst kurzreichweitig geordneten $Fe_{60}V_{40}$-Legierungsfilms Ferromagnetismus erzeugt. Unabhängig vom Pfad der Gitter(un)ordnung kann Ferromagnetismus entweder durch Ionenbestrahlung oder durch einzelne Femtosekunden-Laserpulse ausgelöst werden. Die ferromagnetischen Bereiche sind somit räumlich auf die jeweiligen Ionen-/Photonen-Materie-Wechselwirkungsvolumina beschränkt.

Es ergibt sich ein umfassendes Bild, in dem verschiedene Wege zur Realisierung ferromagnetischer Ordnungsstrukturen für Anwendungen wie magnetische Musterbildung im Nanomaßstab und Spintransport genutzt werden können. Darüber hinaus werden grundlegende Erkenntnisse zum Zusammenhang zwischen atomarer und magnetischer Ordnungsbildung gewonnen. Diese geben Impulse zur Entwicklung weiterer Legierungssysteme für die magnetische Manipulation durch atomare Verschiebungen.

3 Progress Report

Ferromagnetic onsets can be realized in non-ferromagnetic alloys through atomic displacements. In the preceding DFG funded project, MUMAGI, ferromagnetic onsets in the paramagnetic B2 $Fe_{60}Al_{40}$ as well as antiferromagnetic B2 $Fe_{50}Rh_{50}$ alloys were explored through observations primarily of the magnetic behaviour. The outcomes provided the basis for MUMAGI II, where the scope of the investigations was broadened to ferromagnetic onset emerging from a different mechanism, namely, lattice ordering due to atomic displacements. The prototype system, demonstrated within this project, is the $Fe_{60}V_{40}$ alloy. Here lattice ordering within the initially paramagnetic short-range ordered alloy is induced through atomic displacements, leading to the onset of ferromagnetism **[Anwa2022]**.

Taken together, the three prototype systems named above provided a tool-kit for the manipulation of magnetism and transport through variations to the lattice order. Changes to the lattice order have been confined to the nanoscale, through focussed ions as well as femtosecond laser beams, thereby providing a convenient, commercially applicable, path to the production of nanoscale magnets and magnetic modulations. The scope of MUMAGI II can be sub-divided into three major research lines: i) understanding ferromagnetic onsets through spectroscopy, ii) producing nanoscale magnetic modulations iii) tracking transport properties during the ferromagnetic onset. A further category iv) other associated outcomes, that were not anticipated at the time of proposal, will also be discussed.

The HZDR and UDE teams collaborated closely on all of the above. The research lines are indeed interlinked; thus, a continuous exchange of knowhow was necessary and could be maintained through regular meetings, both online and in-person as well as joint beamtimes at synchrotron sources (BESSY, PETRA) as well as at the ELBE and Ion Beam Centre facilities of the HZDR. Thin-films preparation as well as ion-irradiation were performed by the HZDR team. The spectroscopy investigations, in particular using the EXAFS and XMCD techniques were led by the UDE team. Part of the thin-films preparation ($Fe_{50}Rh_{50}$) as well as theoretical inputs were obtained through external collaborations, including Prof. Thomas Thomson (Manchester University, UK) and Prof. Yanning Zhang (UESTC, China). Selected outcomes of MUMAGI II are described below:

i) Understanding ferromagnetic onsets through spectroscopy

Ferromagnetic onsets provide a wide variety of options for spectroscopic investigations. Observations of the local Fe – and V- environments during the lattice re-ordering of short-range ordered $Fe_{60}V_{40}$ revealed that with increasing atomic displacements, formation of the Fe sub-lattice is shown to precede the V sub-lattice **[Raul2024]**. These insights were achieved using extended X-ray absorption fine structure (EXAFS) spectroscopy at the Fe and V K-edges. Measurements were led by the UDE group at the PETRA III synchrotron facility's beamline P65. Samples consisting of 40 nm thick $Fe_{60}V_{40}$ films grown on SiO_2 buffered Si substrates were prepared by magnetron sputtering by the HZDR group. Films were grown at 300 K as well as at 573 K, to obtain different initial states of short-range ordering. Ion-irradiation using a broad-beam of 25 keV Ne^+-ions at varying fluences was performed at the Ion Beam Centre of the HZDR, to produce a sample set where the short-range ordered $Fe_{60}V_{40}$ gradually transforms to the BCC phase (Fig. 1, schematic). In addition to the local environments, the presence of mono-vacancies was confirmed, and their evolution with increasing atomic displacements probed using positron annihilation performed at the HZDR.

The difference in the local environments of the fully transformed, BCC $Fe_{60}V_{40}$ and the SRO $Fe_{60}V_{40}$ films is immediately apparent in the EXAFS spectra (Fig. 1a), where the BCC structure leads to well-defined intensity oscillations, over a wide photon energy range. Oscillations observed on the as-grown $Fe_{60}V_{40}$ film indicates the presence of SRO. The oscillations in the energy spectrum can be analyzed by plotting the k-weighted spectral lines (Fig. 1b – d) during various stages of the SRO to BCC transition. Fourier transforms of the k-weighted spectra (Fig. 1e - g) yields the real-space distribution of resonances centered around the Fe and V atoms. The experimental observations are replicated by starting with approximate models of the system and calculating the resulting spectra which is feedback for refining the structural model, thus converging to the local structure of the $Fe_{60}V_{40}$ alloy during the lattice ordering.

The above observations revealed that the final lattice ordering in $Fe_{60}V_{60}$ depends on the initial degree of SRO, which varies with the growth temperature. Fewer atomic displacements are necessary to generate lattice ordering in the films grown at 573 K, compared to the films grown at 300 K. In a separate study, films grown at 573 K possess a higher saturation magnetization, M_s, than those grown at 300 K, after correcting for the BCC volume **[Anwa2022]**. EXAFS measurements show that the BCC structure of the 573 K grown films possesses a higher degree of ordering and is consistent with the higher M_s. Furthermore, the 573 K grown films are more sensitive to atomic displacements forming the BCC lattice at lower ion-fluences, confirmed by the EXAFS. Intriguing differences in the rates of Fe- and V- sub-lattices were observed, as a step towards understanding the mechanism of the SRO to BCC transition.

In addition to the effect of atomic displacements, the effect of alloy composition has also been experimentally investigated. Films were prepared using molecular beam epitaxy at the UDE

group, where an enriched ^{57}Fe source was used, for enhancing the Mössbauer intensity. Figure 2 shows results of conversion electron Mössbauer spectroscopy (CEMS) on $Fe_{1-x}V_x$ alloys with x varied in steps of 0.1 or lower. As x is increased, the sextet of lines due to hyperfine splitting continues to be observed before vanishing at x = 0.4 (Fig. 2a). Analysis of the sextet intensities shows a gradually decreasing hyperfine field, B_{HF}, that shows a sharp decrease between x = 0.35 and x = 0.4 (Fig. 2b). The isomer shift (IS) can be extracted for all spectra, showing a negative value that linearly decreases with increasing x, however deviating from the linear trend, for 0.35 < x < 0.6 (Fig. 2c). In this range, corresponding to the presence of SRO Fe-V the IS values fall even lower than the linear trend. The pronounced negative IS suggest an increased electron density surrounding the ^{57}Fe nuclei in the SRO regime.

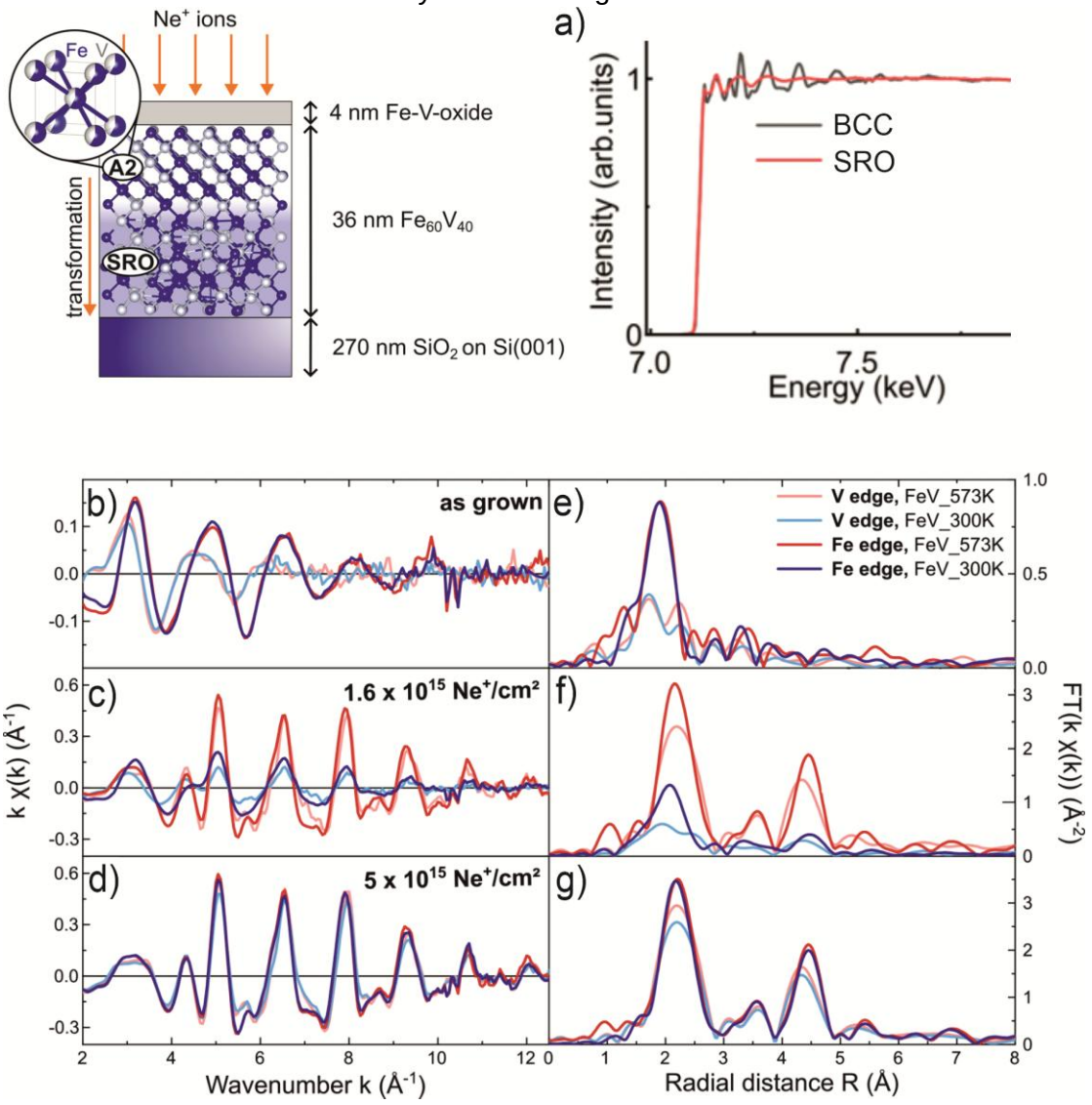

Figure 1: Short-range order (SRO) to body-centred-cubic (BCC) transformation under ion-irradiation, shown schematically on the top-left. a) Extended X-ray absorption fine structure (EXAFS) of the SRO and BCC $Fe_{60}V_{40}$ films at the Fe K-edge. The as-grown 40 nm thick $Fe_{60}V_{40}$ films are short-range ordered, and were irradiated with Ne^+-ions at 25 keV. The k-weighted spectral lines (b - d) are shown for $Fe_{60}V_{40}$ films, grown at 300 and 573 K and irradiated with increasing ion-fluences. The corresponding Fourier transforms are shown in e -g). Adapted from **[Raul2024]**.

Spectroscopic probing of ferromagnetic onsets in the other prototype alloys were also pursued, following the same working-structure as above, with the UDE group in the lead. Observations of the local environment during the lattice disordering of B2 $Fe_{60}Al_{40}$ were reported within the

previous funding round. In MUMAGI II, the spectroscopic investigations were pursued using X-ray Circular Magnetic Dichrosim (XMCD) **[Smek2024]** as well as Nuclear Resonant Reflectivity (NRR) **[Andr2021]**.

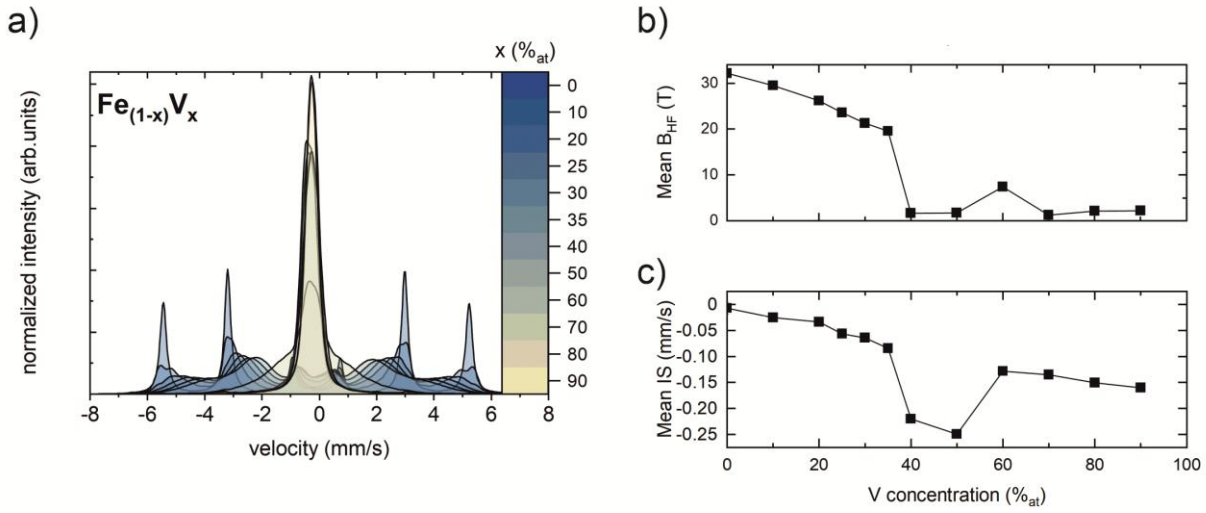

Figure 2: Composition dependence of Mössbauer spectra in $Fe_{1-x}V_x$ films grown using MBE. a) The CEMS spectra as a function of *x*, showing the evolution of the sextet (*x* = 0) to a single absorption line for *x* > 0.4. The composition dependence of the hyperfine field (b) and the isomer-shift (c) are shown [S. Rauls *et al.*, *in preparation*].

ii) Producing nanoscale magnetic modulations over large areas

Ferromagnetic onsets can be exploited to produce nanoscale magnetic modulations as well as nanoscale single objects. This was realized by ion-irradiation at the HZDR, on thin films covered with shadow masks. Two different types of shadow masks were applied, a) resist masks prepared by e-beam lithography and b) self-assembled polystyrene nanospheres as shadow masks. The schematic in Figure 3 depicts the resist masks prepared using e-beam lithography at Manchester University. Here, B2 $Fe_{50}Rh_{50}$ was selected since it shows a transition from the initial antiferromagnetic state to the ferromagnetic as the temperature exceeds 380 K. The system returns to antiferromagnetic state upon cooling. On the other hand, small atomic displacements causing static disorder in the B2 structure leads to a ferromagnetic onset that is non-volatile. The ion-energies and fluence were selected such that the ferromagnetic onset is homogeneously distributed through the full 36 nm thickness of the film, based on a previous work performed using broad-beam ion-irradiation and polarized neutron reflectivity observations **[Grig2020]**.

Deploying a shadow mask in the form of 100 nm wide resist stripes, separated by 100 nm wide spacings, a combination of the temperature driven metamagnetic transition as well as the ferromagnetic onset were realized on the same chip **[Grig2025]**. The B2 $Fe_{50}Rh_{50}$ covered with the resist mask was irradiated at the HZDR by 25 keV Ne^+ ions at a fluence of 7.5×10^{13} ions cm^{-2}.

As seen in the magnetic force microscopy images of Fig. 3a and b, at 299 K, stray-fields are emergent only from the 100 nm wide regions penetrated by the Ne^+-ions. Stray fields are present throughout the sample surface at 433 K i.e., above the transition temperature where the shadowed regions show the antiferromagnetic to ferromagnetic transition. Observations of the magnetization were made using spin-polarized X-ray photoemission electron microscopy, carried out at the BESSY II synchrotron facility. The ferromagnetic stripes are clearly observed, forming domains with magnetization, **m**, largely parallel to the stripes, where the red (blue)

contrast indicates **m** parallel (anti-parallel) to the incident circularly polarized X-ray beam (Fig. 3c). As the temperature is increased to 470 K, the stripe-like contrast is suppressed (Fig. 3d). Cooling to below the metamagnetic transition temperature returns the stripe-like magnetic contrast (Fig. 3e). Thus a temperature reversible nanoscale magnetic modulation over large areas is demonstrated.

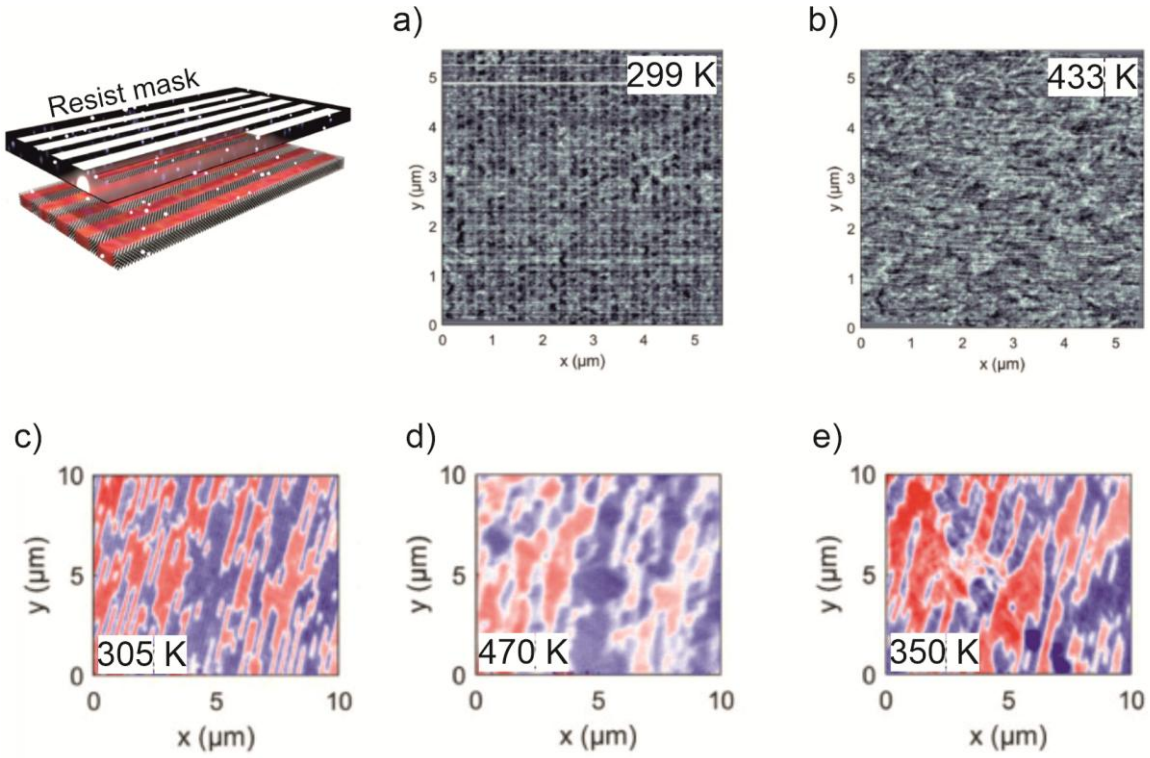

Figure 3: Magnetic pattering of B2 $Fe_{50}Rh_{50}$. Static disorder is generated locally by irradiating through a resist mask (top left). a) Magnetic modulations of 100 nm periodicity are observed in the stray-field contrast obtained using magnetic force microscopy (MFM). The irradiated regions are ferromagnetic, whereas the shadowed regions are antiferromagnetic. b) The magnetic modulations vanish at elevated temperatures as the antiferromagnetic stripes undergo a metamagnetic phase transition, becoming ferromagnetic. c) Imaging the magnetization, **m**, contrast (as opposed to stray fields shown in a and b), where the magnetization of the red (blue) regions are parallel (anti-parallel) to an incident beam of circularly polarized X-rays at the Fe $L_{2,3}$ edge. d) The modulations of the **m** contrast vanishing at elevated temperatures and e) reappearing during cooling. Adapted from **[Grig2025]**.

Shadow masks can also be generated using other methods, for instance using a self-assembled single layer of polystyrene nanospheres (Nanosphere Lithography). This technique was applied to 40 nm thick B2 $Fe_{60}Al_{40}$ **[Zarz2024]**. Polystyrene nanospheres contained in droplets of a carrier solution self-assemble in a hexagonal pattern on the film surface, as the carrier solution evaporates, performed by colleagues at the IFJ PAN in Poland. The size of the nanospheres can be adjusted by subsequent O-plasma etching, thereby giving a masking pattern of isolated magnetic regions to connected antidots are formed. The films covered by the shadow masks were irradiated with Ne^+-ions at energies adjusted for the nanosphere diameters. Regions penetrated by the Ne^+-ions undergo a ferromagnetic onset due to the formation of the chemically disordered A2 $Fe_{60}Al_{40}$. Here, the emphasis was to observe the slow dynamics of magnetic modulations at low-temperatures, and an exchange spring effect of the ferromagnetic regions as well as spin-glass like behavior of the B2 $Fe_{60}Al_{40}$ is revealed.

By using a ~ 2 nm diameter Ne^+-beam of a gas-field ion-source, available at the HZDR, individual magnetic structures can be directly written in a 1-step exposure. In this way a 5 µm × 1

μm ferromagnetic stripe on a B2 $Fe_{60}Al_{40}$ disc placed within a micro-resonator **[Cans2022]**. The focused 25 keV Ne^+-beam was rastered over the the 40 nm thick film to reach fluences of 10 ions.nm^{-2}, to generate ferromagnetic A2 $Fe_{60}Al_{40}$. After measuring the dynamics at 14 GHz, the chemically ordered region was milled away using Ne^+-ions at 15 keV and high fluences of 7500 ions.nm^{-2}, to produce a freestanding ferromagnetic stripe. The resonance of the free-standing and embedded ferromagnetic structures were compared, to identify an anisotropy component due to the B2 ordered lattice surrounding the A2 structure.

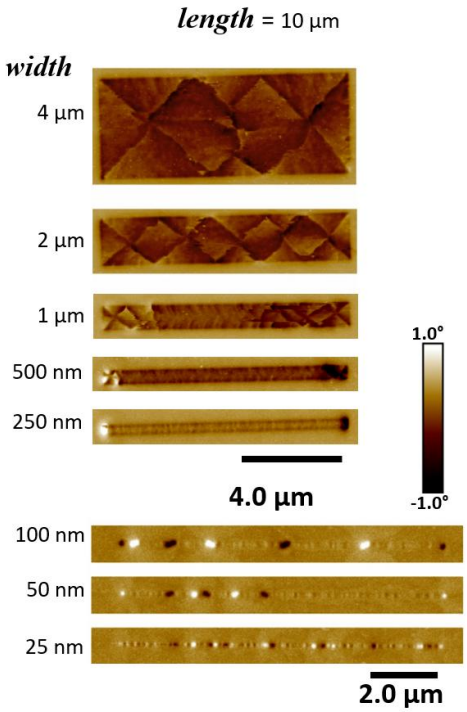

Figure 4: Magnetic writing on SRO $Fe_{60}V_{40}$. A focussed beam of Ne^+-ions at 25 keV is used to locally generate BCC $Fe_{60}V_{40}$, thus writing magnetic stripes of 10 mm lengths and widths varying from 4 mm down to 25 nm, as indicated. The contrast indicates the out-of-plane stray fields. The narrowest stripes in the bottom panel show regions of strong perpendicular stray fields, due to the formation of domain walls. The colour-scale indicates phase-contrast due to the stray-fields [S. Anwar et al., in preparation].

The 1-step writing process can also be applied to SRO $Fe_{60}V_{40}$, as shown in Fig. 4. Ferromagnetic stripes of 10 μm lengths and widths of 4 μm down to 25 nm, by rastering a 25 keV Ne^+ beam at fluences of 50 ions.nm^{-2}. A geometry dependent evolution of the domain pattern is observed in the stray-field contrast, with the wider stripes forming a Landau-like pattern. As the width is narrowed, a tendency to form a single domain structure with magnetic poles at each end is observed. However, in the narrowest stripes, domains with strong perpendicular stray-fields are found, which can be applications relevant. Furthermore, a single femtosecond laser pulse also produces ferromagnetic onsets. The changes to the lattice ordering occur through a different path *viz.* melting and rapid cooling to form chemical disorder in B2 $Fe_{60}Al_{40}$ as well as structural order in SRO $Fe_{60}V_{40}$ **[Pflu2024]**. This opens a new area for research, where magnetic modulations can be achieved through laser pulsing.

iii) Tracking transport properties during the ferromagnetic onset

Transport properties can be highly sensitive to lattice ordering, and this was investigated for the case of B2 $Fe_{60}Al_{40}$. During the early stages of the disordering, the regions possessing the ferromagnetic onset are spatially inhomogeneous, rendering a sparse regime of ferromagnetic defects distributed within a paramagnetic matrix. Further disordering leads to the coalescence of the ferromagnetic regions. The lattice remains conducting throughout the disordering process, however the electron scattering is likely to be sensitive to the distribution of the ferromagnetic regions. This raises the question, does the electron scattering in the sparse regime due to the structural defects *i.e.* lattice disorder alone, and therefore spin-independent, or a spin-dependent electron scattering is present?

A mesoscopic Hall bar of B2 $Fe_{60}Al_{40}$ was patterned onto an SiO_2 buffers, and the resistivity, and the anomalous Hall effect (AHE), were tracked in situ irradiation with a focussed Ne^+-ion beam (Fig. 5) **[Soro2023]**. A home-built sample holder with a permanent magnet was used, such that a perpendicular magnetic field of 400 mT was present during the measurement. Electrical probes arranged in the 4-probe as well as Hall geometry were used to measure the resistivity ρ_{xx} as well as the Hall resistivity, ρ_{xy}, respectively. The experiments show an

unambiguous peak of ρ_{xx} as well as ρ_{xy} observed during the early stages of chemical disordering (Fig. 5a). The peak observed in the AHE provides clear indication of the electron scattering occurring due to the local magnetic moments of the disordered regions. The increase of the ρ_{xy} vs. ρ_{xx} behaviour during the initial disordering (Fig. 5b) suggests an increasing defect concentration, and subsequent slope reversal (corresponding to the resistivity peaks) tends towards a clean material, indicating the coalescence of the disordered defect regions.

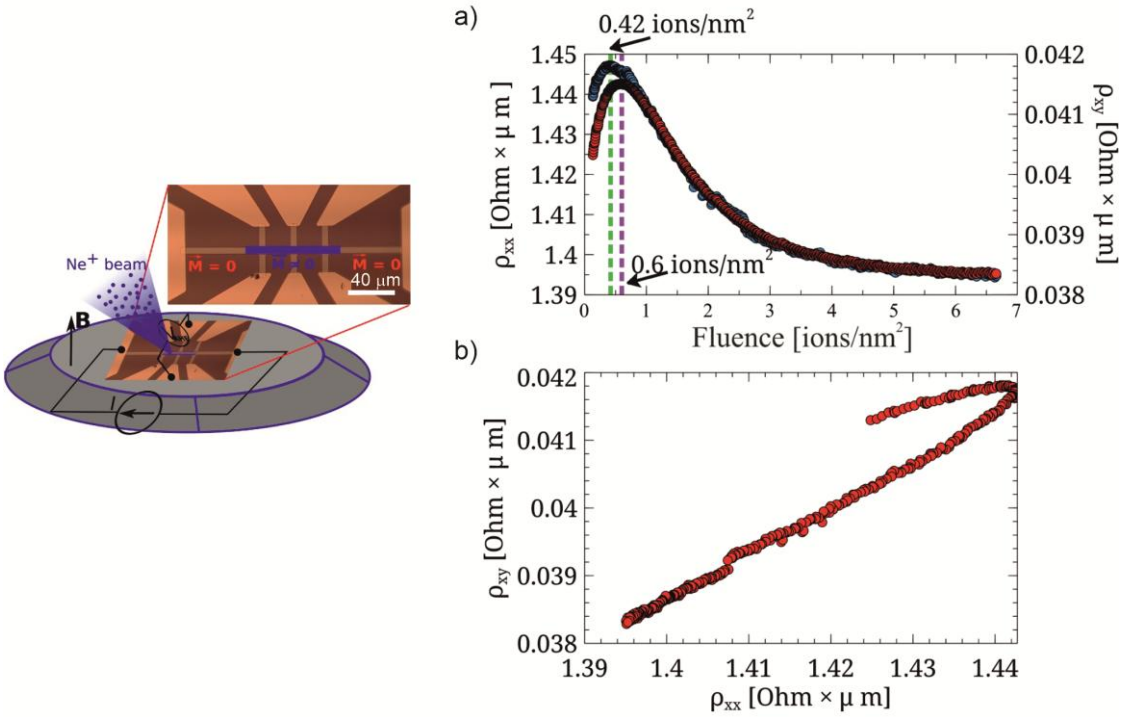

Figure 5: In situ observations of transport properties in disordered $Fe_{60}Al_{40}$. The set-up is depicted on the left. A mesoscopic wire of B2 $Fe_{60}Al_{40}$ was irradiated with a focussed beam of Ne^+ ions at 25 keV. a) The resistivity ρ_{xx} and anomalous Hall effect (ρ_{xy}) as functions of Ne^+ ion fluence. b) Resistivity vs. AHE for the data shown in a).

Relevant to applications, the fully disordered A2 $Fe_{60}Al_{40}$ can be reordered to the B2 structure via Joule heating, by increasing the current density. This implies that the material may be useful for sensing applications, for instance to detect cosmic particles, and returned to the pristine state for repeat measurements. Furthermore, the theoretical prediction of a large spontaneous Hall angle of ~ 3 % [Kudrnovsky *et al.*, *Phys. Rev.* B **101** 054437] was confirmed using Andreev reflection, performed at the Trinity College Dublin **[Bori2021]**. The spin-pumping applications of $Fe_{60}Al_{40}$ were also demonstrated **[Strus2022]**.

iv) Other associated outcomes

Research lines i – iii) closely follow the objectives proposed in MUMAGI II. Further research outcomes, are summarized below. Detailed investigation of the ferromagnetic onset in the $Fe_{60}V_{40}$ system formed the basis of a finished PhD thesis **[Anwa2022a]**. An ongoing PhD thesis gives further insights into the changes of the local Fe and V environments during lattice reordering [S. Rauls, in preparation]. Ferromagnetic onsets due to lattice disorder are the subject of a book chapter **[Bali2020]**. The atomic displacements preserve the flat film topography, while generating ferromagnetic regions within the film. This makes these samples highly amenable for advanced transmission electron microscopy methods, such as differential phase contrast (DPC) imaging. The absence of topographical edges simplifies the comparison of the phase shift due to the sample magnetization to that of the direct beam. The nanocrystalline

structure of the films provides near-ideal samples for the developments and tests of DPC methods, aimed at separating the magnetic information in the presence of diffraction **[Nord2025] [Nord2025a]**. Refinements of micro-resonators, so as to compare the ferromagnetic resonance of freestanding and embedded objects were also realized during the project **[Cans2021]**.

4 Published Project Results

4.1 Publications with scientific quality assurance

- **[Andr2021]**: Andreeva, M., Smekhova, A., Baulin, R., Repchenko, Y., Bali, R., Schmitz-Antoniak, C., Wende, H., Sergueev, I., Schlage, K., Wille, H. C.
  Evolution of the magnetic hyperfine field profiles in ion-irradiated $Fe_{60}Al_{40}$ film measured by nuclear resonant reflectivity
  Journal of Synchrotron Radiation 28(2021), 1535-1543.
  10.1107/S1600577521007694
- **[Anwa2022]**: Anwar, M. S., Cansever, H., Boehm, B., Gallardo, R., Hübner, R., Zhou, S., Kentsch, U., Rauls, S., Eggert, B., Wende, H., Potzger, K., Faßbender, J., Lenz, K., Lindner, J., Hellwig, O., Bali, R.
  Depth-Adjustable Magnetostructural Phase Transition in $Fe_{60}V_{40}$ Thin Films
  ACS Applied Electronic Materials 4(2022)8, 3860-3869.
  10.1021/acsaelm.2c00499
- **[Bori2021]**: Borisov, K., Ehrler, J., Fowley, C., Eggert, B., Wende, H., Cornelius, S., Potzger, K., Lindner, J., Faßbender, J., Bali, R., Stamenov, P.
  Spin polarization and magnetotransport properties of systematically disordered $Fe_{60}Al_{40}$ thin films
  Physical Review B 104(2021), 134417.
  10.1103/PhysRevB.104.134417
- **[Cans2022]**: Cansever, H., Anwar, M. S., Stienen, S., Lenz, K., Narkovic, R., Hlawacek, G., Potzger, K., Hellwig, O., Faßbender, J., Lindner, J., Bali, R.
  Resonance behavior of embedded and freestanding microscale ferromagnets
  Scientific Reports 12(2022), 14809.
  10.1038/s41598-022-15959-0 (Open Access)
- **[Grig2025]**: Griggs, W., Peasey, A., Schedin, F., Anwar, M. S., Eggert, B., Mawass, M.-A., Kronast, F., Wende, H., Bali, R., Thomson, T.
  Magnetic imaging of thermally switchable antiferromagnetic/ferromagnetic modulated thin films
  Acta Materialia 283(2025), 120515.
  10.1016/j.actamat.2024.120515 (Open Access)
- **[Grig2020]**: Griggs, W., Eggert, B., Liedke, M. O., Butterling, M., Wagner, A., Kentsch, U., Hirschmann, E., Grimes, M., Caruana, A. J., Kinane, C., Wende, H., Bali, R., Thomson, T.
  Depth selective magnetic phase coexistence in FeRh thin films
  APL Materials 8(2020)12, 121103.
  10.1063/5.0032130 (Open Access)
- **[Pflu2024]**:Pflug, T., Pablo-Navarro, J., Anwar, M. S., Olbrich, M., Magén, C., Ibarra, M. R., Potzger, K., Faßbender, J., Lindner, J., Horn, A., Bali, R.
  Laser-Induced Positional and Chemical Lattice Reordering Generating Ferromagnetism
  Advanced Functional Materials 34(2024)13, 2311951.
  10.1002/adfm.202311951 (Open Access)
- **[Raul2024]**: Rauls, S., Anwar, M.S., Liedke, M. O., Butterling, M., Eggert, B., Welter, E., Günzing, D., Klaßen, P., Herman, A., Hellwig, O., Fassbender, J., Lindner, J., Wagner, A., Potzger, K., Bali, R., Wende, H.

Evolution of defects and local environment during the magneto-structural phase transition in $Fe_{60}V_{40}$ thin films
Physical Review Materials 8(2024)11, 114415.
10.1103/PhysRevMaterials.8.114415

- **[Smek2024]**: Smekhova, A., Szyjka, T., La Torre, E., Ollefs, K., Eggert, B., Cöster, B., Wilhelm, F., Bali, R., Lindner, J., Rogalev, A., Többens, D., Weschke, E., Luo, C.; Chen, K., Radu, F., Schmitz-Antoniak, C., Wende, H.
Irradiation-induced enhancement of Fe and Al magnetic polarizations in $Fe_{60}Al_{40}$ films
New Journal of Physics 26(2024), 023036.
10.1088/1367-2630/ad1497 (Open Access)
- **[Soro2023]**: Sorokin, S., Anwar, M. S., Hlawacek, G., Boucher, R., Salgado Cabaco, J., Potzger, K., Lindner, J., Faßbender, J., Bali, R.
Transport properties of $Fe_{60}Al_{40}$ during the B2 to A2 structural phase transition
New Journal of Physics 25(2023), 093036.
10.1088/1367-2630/acdf13 (Open Access)
- **[Strus2022]**: Strusch, T., Lenz, K., Meckenstock, R., Bali, R., Ehrler, J., Lindner, J., Faßbender, J., Farle, M., Potzger, K., Semisalova, A.
Spin pumping at interfaces with ferro- and paramagnetic $Fe_{60}Al_{40}$ films acting as spin source and spin sink
Journal of Applied Physics 132(2022), 213906.
10.1063/5.0125699 (Open Access)
- **[Zarz2024]**: Zarzycki, A., Anwar, S., Bali, R., Potzger, K., Krupinski, M., Marszalek, M.
Identifying magnetic phases in chemically ordered and disordered FeAl thin films
RSC Advances 14(2024), 36763-36770.
10.1039/D4RA06100D (Open Access)

4.2 Other publications and published results

- **[Anwa2022a]**: Anwar, Md. S., Magnetostructural Phase Transition in $Fe_{60}V_{40}$ Thin Films, Dissertation (TU Dresden, 2022).
- **[Bali2020]**: Bali, R.
Book Chapter: Ferromagnetism in B2-Ordered Alloys Induced via Lattice Defects
Francis Chi-Chung Ling, Shengqiang Zhou, Andrej Kuznetsov: Defects in Functional Materials, Hong Kong: World Scientific Publishing Co Pte Ltd, 2020, 978-981-120-316-9, 201-239.
10.1142/11352
- **[Cans2021]**: Cansever, H., Lindner, J.
Microresonators and Microantennas—tools to explore magnetization dynamics in single nanostructures
Magnetochemistry 7(2021)2, 28.
10.3390/magnetochemistry7020028 (Open Access)
- **[Nord2025]**: Nordahl, G., Dagenborg, S., D'Alessio, A., Brand, E., Vitaliti, N., Trier, F., Park, D., Pryds, N., Sørhaug, J., Nord, M.
On the effect of precession for magnetic differential phase contrast imaging
Micron 190 (2025), 103761.
10.1016/j.micron.2024.103761
- **[Nord2025a]**: Nordahl, G., Dagenborg, S., Sørhaug, J., Nord, M.
Exploring deep learning models for 4D-STEM-DPC data processing
Ultramicroscopy 267 (2024), 114058.
10.1016/j.ultramic.2024.114058

4.3 Patents (applied for and granted)

no patents

Further information on the project, qualifications and outlook

The exploration of ferromagnetic onsets commenced with the first MUMAGI project in 2017. The main outcomes included: 1) Observations of the correlation between chemical disorder, lattice parameter and M_s in B2 $Fe_{60}Al_{40}$, 2) ferromagnetic onset driven by single femtosecond laser pulses on $Fe_{60}Al_{40}$ as well as B2 $Fe_{50}Rh_{50}$, 3) preliminary observations of the sensitive dependence of transport properties on chemical disorder in B2 $Fe_{60}Al_{40}$ and 4) preliminary observations of the ferromagnetic onset in SRO $Fe_{60}V_{40}$. The list of publications of MUMAGI is as follows:

1. J. Ehrler, B. Sanyal, B. Eggert, J. Grenzer, S. Zhou, R. Böttger, H. Wende, J. Lindner, J. Fassbender, C. Leyens, K. Potzger, R. Bali
   Magneto-structural correlations in a systematically disordered B2 lattice
   New J. Phys. 22, 073004 (2020).

2. B. Eggert, A. Schmeink, J. Lill, M. O. Liedke, U. Kentsch, M. Butterling, A. Wagner, S. Pascarelli, K. Potzger, J. Lindner, T. Thomson, J. Fassbender, K. Ollefs, W. Keune, R. Bali, H. Wende
   Magnetic response of FeRh to static and dynamic disorder
   RSC Adv. 10, 14386-14395 (2020).

3. J. Ehrler, M. O. Liedke, J. Čížek, R. Boucher, M. Butterling, S. Zhou, R. Böttger, E. Hirschmann, T. T. Trinh, A. Wagner, J. Lindner, J. Fassbender, C. Leyens, K. Potzger, R. Bali
   The role of open-volume defects in the annihilation of antisites in a B2-ordered alloy
   Acta Mater. 176, 167 (2019).

4. M. Nord, A. Semisalova, A. Kákay, G. Hlawacek, I. Maclaren, V. Liersch, O. M. Volkov, D. Makarov, G. W. Paterson, K. Potzger, J. Lindner, J. Fassbender, D. McGrouther, R. Bali
   Strain anisotropy and magnetic domains in embedded nanomagnets
   Small 1904738 (2019).

5. T. Schneider, K. Lenz, A. Semisalova, J. Gollwitzer, J. Heitler-Klevans, K. Potzger, J. Fassbender, J. Lindner, R. Bali
   Tuning ferromagnetic resonance via disorder/order interfaces
   J. Appl. Phys. 125 (19), 195302 (2019).

6. M. Krupinski, R. Bali, D. Mitin, P. Sobieszczyk, J. Gregor-Pawlowski, A. Zarzycki, R. Böttger, M. Albrecht, K. Potzger, M. Marszałek

Ion induced ferromagnetism combined with self-assembly for large area magnetic modulation of thin films
Nanoscale 11 (18), 8930 (2019).

7. F. Hammerath, R. Bali, R. Hübner, M.R.D. Brandt, S. Rodan, K. Potzger, R. Böttger, Y. Sakuraba, S. Wurmehl
Structure-property relationship of Co2MnSi thin films in response to He^+-irradiation
Sci. Rep. 9 (1), 2766 (2019).

8. E. La Torre, A. Smekhova, C. Schmitz-Antoniak, K. Ollefs, B. Eggert, B. Cöster, D. Walecki, F. Wilhelm, A. Rogalev, J. Lindner, R. Bali, R. Banerjee, B. Sanyal, H. Wende
Local probe of irradiation-induced structural changes and orbital magnetism in thin films via an order-disorder phase transition
Phys. Rev. B 98 (2), 024101(2018).

9. J. Ehrler, M. He, M.V. Shugaev, N.I. Polushkin, S. Wintz, V. Liersch, S. Cornelius, R. Hübner, K. Potzger, J. Lindner, J. Fassbender, A.A. Ünal, S. Valencia, F. Kronast, L. V. Zhigilei, R. Bali
Laser-rewriteable ferromagnetism at thin-film surfaces
ACS Appl. Mater. Interfaces 10 (17), 15232-15239 (2018).

10. A. Heidarian, S. Stienen, A. Semisalova, Y. Yuan, E. Josten, R. Hübner, S. Salamon, H. Wende, R. A. Gallardo, J. Grenzer, K. Potzger, R. Bali, S. Facsko, J. Lindner
Ferromagnetic resonance of MBE-grown FeRh thin films through the metamagnetic phase transition
Phys. Status Solidi B 254, 10, 1700145 (2017).